Atmos. Chem. Phys. Discuss., 13, 2759–2793, 2013
www.atmos-chem-phys-discuss.net/13/2759/2013/
doi:10.5194/acpd-13-2759-2013

Atmospheric Chemistry and Physics Discussions

Modeling organic aerosol from the oxidation of α-pinene in a Potential Aerosol Mass (PAM) chamber

S. Chen[1], W. H. Brune[1], A. Lambe[2,3], P. Davidovits[2], and T. Onasch[2,3]

[1]Department of Meteorology, Pennsylvania State University, University Park, PA, USA
[2]Chemistry Department, Boston College, Chestnut Hill, MA, USA
[3]Aerodyne Research Inc., Billerica, MA, USA

Received: 9 January 2013 – Accepted: 17 January 2013 – Published: 25 January 2013

Correspondence to: S. Chen (suc185@psu.edu)

Published by Copernicus Publications on behalf of the European Geosciences Union.

Abstract

A model has been developed to simulate the formation and evolution of secondary organic aerosol (SOA) and was tested against data produced in a Potential Aerosol Mass (PAM) flow reactor and a large environmental chamber. The model framework is based on the two-dimensional volatility basis set approach (2D-VBS), in which SOA oxidation products in the model are distributed on the 2-D space of effective saturation concentration (C_i^*) and oxygen-to-carbon ratio (O : C). The modeled organic aerosol mass concentrations (C_{OA}) and O : C agree with laboratory measurements within estimated uncertainties. However, while both measured and modeled O : C increase with increasing OH exposure as expected, the increase of modeled O : C is rapid at low OH exposure and then slows as OH exposure increases while the increase of measured O : C is initially slow and then accelerates as OH exposure increases. A global sensitivity analysis indicates that modeled C_{OA} values are most sensitive to the assumed values for the number of C_i^* bins, the heterogeneous OH reaction rate coefficient, and the yield of first-generation products. Modeled SOA O : C values are most sensitive to the assumed O : C of first-generation oxidation products, the number of C_i^* bins, the heterogeneous OH reaction rate coefficient, and the number of O : C bins. All these sensitivities vary as a function of OH exposure. The sensitivity analysis indicates that the 2D-VBS model framework may require modifications to resolve discrepancies between modeled and measured O : C as a function of OH exposure.

1 Introduction

Organic aerosols (OA) play an important role in environmental processes through their impact on climate and human health (EPA, 2012). A significant fraction of the OA is the secondary organic aerosols (SOA) (Yu et al., 2007), which are produced by the gas-to-particle conversion of semi-volatile oxidation products of volatile organic compounds (VOCs). However, the formation and continued oxidation of SOA involve a great number

ACPD
13, 2759–2793, 2013

of complex physical and chemical processes, of which a quantitative and predictive understanding remains a major research challenge (Hallquist et al., 2009).

Great effort has been made to simulate the formation of SOA through different modeling approaches. Following the absorptive partitioning theory of Pankow (Pankow, 1994), a partitioning coefficient of a given species, K_p, was defined to describe the thermodynamic equilibrium of the species between gas-phase and condensed-phase. With detailed gas-phase reaction mechanisms, the formation of SOA can be modeled in an explicit way while the gas-to-particle transfer reactions are defined for all semi-volatile reaction products. Unfortunately, a full explicit mechanism of SOA precursor oxidation is currently not practical since it would contain an unmanageable number of chemical reactions and intermediate species (Aumont et al., 2005). Odum et al. (1996) developed a two-product model, which is simply parameterized by laboratory-derived mass yields and partitioning coefficients for two surrogate compounds and hence cannot represent the complexity of the SOA system (Hallquist et al., 2009).

Donahue et al. (2006) and Robinson et al. (2007) proposed the Volatility Basis Set (VBS) model framework to model SOA with only a few model parameters by lumping the oxidation products according to their volatility. The VBS framework distributes all organic species into volatility bins with discrete values of effective saturation concentration C_i^*, separated by factors of 10. The mass yields for each bin α_i can be parameterized by fitting the data from chamber experiments for a selection of C_i^* values (Stanier et al., 2008). In addition to the mass and volatility, other properties of organic material such as hygroscopicity, polarity, and carbon number evolve with photochemical processing. To characterize the atmospheric evolution of SOA, Jimenez et al. (2009) and Donahue et al. (2011) developed a 2D-VBS model framework by using oxygen-to-carbon atomic ratio (O : C) as the second dimension. The organic products are hence classified by both C_i^* and O : C and their evolution can be mapped on the 2-D space through the variations of volatility and oxidation state resulting from two chemical reaction processes: functionalization and fragmentation. Functionalization refers

ACPD
13, 2759–2793, 2013

to a net addition of oxygen without change of carbon number by adding oxygenated functional groups to a reactant, moving the products to lower volatility and higher oxidation states; fragmentation refers to a net loss of carbon due to carbon-carbon bond cleavage, moving the products to higher volatility (Kroll et al., 2011).

An advantage of the VBS model is its treatment of both gas-phase and particle-phase organic compounds into products that are grouped into bins with common chemical behavior. This model has been coupled with different chemistry models (Murphy et al., 2011, 2012a; Roldin et al., 2011) and was found to be a good approximation of ambient SOA formation and chemical aging processes. The 2D-VBS has been shown to provide at least a partial solution to representing the aging mechanism of α-pinene SOA (Donahue et al., 2012a). Recently it was also used to model SOA mass yields from six linear oxygenated precursors (Chacon-Madrid et al., 2012) and showed reasonable agreement with smog-chamber measurements. However, many model parameters are parameterized to describe the kinetic evolution of SOA, the probability of functionalization and fragmentation, the distribution of the oxidation products in the 2-D space, and the configuration of aging processes. These parametrizations may influence the model results (e.g., Lane et al., 2008; Murphy et al., 2011; Cappa and Wilson, 2012). These parametrizations can be examined by testing the 2D-VBS model against more laboratory measurements and by exploring the model uncertainty with a sensitivity study, especially for atmospherically relevant SOA aging.

In the atmosphere, a typical residence time for an aerosol is $\sim$ 1 week (Wagstrom and Pandis, 2009). Conventional smog-chamber techniques cannot reproduce this equivalent level of atmospheric oxidation in the laboratory (e.g. Ng et al., 2010). However, recent measurements suggest that it is possible to simulate atmospheric SOA oxidation in a small, highly reactive, flow-through chamber, such as the Potential Aerosol Mass (PAM) chamber (Kang et al., 2007; Lambe et al., 2011, 2012; Bahreini et al., 2012). In the PAM chamber, SOA is formed and oxidized over integrated exposure times ranging from one day to more than a week of equivalent atmospheric oxidation. Thus the PAM chamber can produce atmospheric levels of oxidation that are not possible in

ACPD
13, 2759–2793, 2013

conventional smog chambers. The PAM chamber therefore provides an opportunity to evaluate the 2D-VBS approach for the evolution of SOA over multiple generations of oxidation.

In this work, we focus on SOA produced from α-pinene, which is the most highly-emitted monoterpene (Guenther et al., 1995). As a result, laboratory α-pinene SOA is commonly used as a surrogate for ambient biogenic SOA, which is thought to dominate the global SOA budget (Hallquist et al., 2009; Spracklen et al., 2011). The experimental measurements of α-pinene SOA mass concentrations (C_{OA}) and O : C in the PAM chamber are used to evaluate simulations from a recently developed 2D-VBS model, which is described herein. The model and PAM measurements are also compared to results from the Caltech environmental chamber (Ng et al., 2007, 2010; Lambe et al., 2011). Model uncertainties are examined by changing model parameters and the sensitivity of the modeled C_{OA} and O : C to the model parameters are assessed with a global sensitivity analysis.

2 Model and measurements

2.1 PAM chamber conditions

A detailed description of the PAM chamber can be found in Lambe et al. (2011). Only a brief summary is presented here. The PAM chamber is a horizontal 13.1 L glass cylindrical chamber (46 cm length × 22 cm diameter) with a small surface-to-volume (SA/V) ratio (0.14 cm^{-1}). To minimize wall interactions in the PAM, flow is sub-sampled from the center of the reactor while the flow near the walls is pumped out through a bypass. Four mercury lamps (BHK Inc.) with peak emission intensity at $\lambda = 254$ nm are mounted inside the chamber. Ozone (O_3) introduced in the PAM is photolyzed to produce excited oxygen ($O(^1D)$), which then reacts with water vapor (relative humidity RH of 20–40 %) to produce OH radicals at levels ranging from $\sim 10^8$ to $\sim 10^{10}$ molec cm^{-3}. The OH exposure was typically measured at 2.0×10^{10} to 2.2×10^{12} molec cm^{-3} s,

ACPD
13, 2759–2793, 2013

roughly corresponding to 0.2–17 days of atmospheric oxidation at an equivalent ambient OH concentration of 1.5×10^6 molec cm^{-3} (Mao et al., 2009).

Thirteen different initial amounts of α-pinene (ΔVOC = 23–833 μg m^{-3}) were introduced in the PAM chamber at room temperature (20–25 °C). One set of measurements was conducted with O_3 ~ 8 ppmv and RH of 20–25 %. The other set of measurements was conducted with O_3 ~ 20 ppmv and RH of 30–40 %. SOA was formed by the gas-phase oxidation of α-pinene followed by homogeneous nucleation and condensational growth. Seed particles were not used. Particle number concentrations were measured with a TSI Scanning Mobility Particle Sizer (SMPS) and Aerodyne compact and high-resolution time-of-flight Aerosol Mass Spectrometers (AMS) (Drewnick et al., 2005; DeCarlo et al., 2006). Since UV lamps lead to temperature increases and hence less SOA formation in the PAM, mass yield corrections of −0.02 per degree K of temperature increase relative to room temperature were applied (Stanier et al., 2007), which typically increases the yields by 10–15 %. Uncertainty in the SOA mass concentration measurements, C_{OA}, is ±25 % (1σ confidence level). The aerosol O : C ratios were determined by elemental analysis (Aiken et al., 2008) with an uncertainty of ±15 % (1σ confidence level) (Massoli et al., 2010). The measured relationship between C_{OA} or O : C and OH exposure are then compared to those from model simulations for the 13 different initial α-pinene amounts.

2.2 SOA model based on 2D-VBS

The SOA model was developed based on the 2D-VBS model coupled with a series of reactions that take place in the PAM chamber. The base-case 2D-VBS scheme used in this work classified the organic products with C_i^* at 298 K of 10^{-5} to 10^4 μg m^{-3},separated by factors of 10 (i.e., 10 bins of volatility, $n_x = 10$) and with O : C of 0.1 to 1.2, linearly separated by 0.1 (i.e., 12 bins of oxygenation, $n_y = 12$). Therefore 120 grouped organic species were defined in the 2-D space.

The inorganic reactions associated with OH, O_3, water vapor, and the intermediates and their rate coefficients were adapted from Sander et al. (2011). The actinic

ACPD
13, 2759–2793, 2013

flux at $\lambda = 254$ nm (Flux254) emitted by the PAM chamber lamps was assumed to be (2–5) $\times 10^{14}$ photons cm^{-2} s^{-1}. The exact modeled Flux254 is not important for this study because, while OH exposure depends on Flux254, C_{OA} and O : C depend almost exclusively on OH exposure, which is used as the independent variable in the following analyses. The photolysis frequencies of O_3, HO_2, and H_2O_2 were approximated by the product of the actinic flux, quantum yields, and absorption cross sections based on Sander et al. (2011). The reaction rate coefficients of the oxidations of α-pinene by OH and O_3 were adapted from Atkinson et al. (2006). A forward finite-difference approach (e.g., Dzepina et al., 2009) was used in the model to calculate the accumulated products. For instance, the concentration variation of α-pinene d[VOC] was approximated by:

$$\frac{d[\mathrm{VOC}]}{\mathrm{d}t} \approx \frac{\Delta[\mathrm{VOC}]}{\Delta t} = \frac{[\mathrm{VOC}]_{t+1} - [\mathrm{VOC}]_t}{\Delta t}$$
$$= -k_{\mathrm{VOC+OH}}[\mathrm{VOC}]_t[\mathrm{OH}]_t - k_{\mathrm{VOC+O_3}}[\mathrm{VOC}]_t[\mathrm{O_3}]_t \quad (1)$$

with a sufficiently small time step dt.

To simulate the formation of the products from the first-generation oxidation by O_3, the mass yields α_i derived by Pathak et al. (2007) from a wide range of smog-chamber data for low NO_x with UV light and dry conditions (Table 1) were used. O : C and molecular weights of most of these initial products (Table 1) were taken from Chan et al. (2009) if available. Otherwise, the model used O : C of 0.45 (as reported in Lambe et al. (2011) for α-pinene SOA at low OH exposure in the PAM chamber) and molecular weight of 150 g mol^{-1} (as estimated in Pathak et al., 2007). For OH oxidation, the model assumes that the products are the same as those from O_3 oxidation of α-pinene. The model also assumes instantaneous absorptive equilibrium with a gas-to-particle partitioning so that the mass fraction in the particle phase in each volatility bin (Donahue et al., 2006) is:

$$\xi_i = \left(1 + \frac{C_i^*}{C_{\mathrm{OA}}}\right) \quad (2)$$

ACPD
13, 2759–2793, 2013

where C_{OA} is the total mass concentration of organic aerosol. The model starts with a very small but nonzero value of initial C_{OA} ($0.1\,ng\,m^{-3}$ as suggested in Kroll et al., 2007) to partition the organic products for the very beginning of the modeling.

All gas-phase products were assumed to react with OH and O_3 at rate coefficients k_{OH_homo} of $1 \times 10^{-11}\,cm^3\,molec^{-1}\,s^{-1}$ and k_{O_3} of $1 \times 10^{-17}\,cm^3\,molec^{-1}\,s^{-1}$, which have been used in previous studies (e.g., Murphy et al., 2011; Roldin et al., 2011; Jathar et al., 2012). For particle-phase OH reactions, the model uses an effective rate coefficient k_{OH_hetero} of $1 \times 10^{-12}\,cm^3\,molecule^{-1}\,s^{-1}$, which is significantly slower than its gas-phase analogue (e.g., Jimenez et al., 2009; Murphy et al., 2011). However, the model uses the same functionalization and fragmentation algorithm for products of heterogeneous reactions as it does for products of gas-phase reactions (Donahue et al., 2012a).

During the oxidation processes, both functionalization and fragmentation reactions affect the volatility and mass of SOA (Kroll et al., 2009; Chacon-Madrid and Donahue, 2011; Lambe et al., 2012). For the functionalization kernel, oxidation products were assumed to take-up 1, 2, or 3 oxygens (Table 2) and hence reduce their volatility by 1–7 decades with separate probabilities (Jimenez et al., 2009; Roldin et al., 2011). Depending on the carbon number n_C of the parent product, which can be estimated by its O : C and C_i^* (Donahue et al., 2011), the change in O : C during the functionalization processes can then be calculated.

For the fragmentation kernel, the fragmentation fraction of the products was assumed to depend on the O : C ratio as

$$\beta = (O : C)^{f_c} \tag{3}$$

where $f_c = 1/6$ (Jimenez et al., 2009). The cleavage site was assumed to take place randomly at any of the carbon bonds with equal probability (e.g., Jimenez et al., 2009). The simplest way to model O : C of the fragments is to assign the same O : C ratio as the parent, such that the products increase in volatility only (Roldin et al., 2011). Their distribution can be estimated by interpolating the carbon number of the fragments

ACPD
13, 2759–2793, 2013

between the two adjacent volatility bins with different carbon numbers. The products with volatilities greater than the highest C_i^* of the model setting were assumed to be completely volatile and their subsequent products were assumed to stay in the gas phase only.

An alternative method to model fragmentation processes assumes that the fragments are more volatile than the reactant and some fragments have higher O : C than the reactants (e.g., Murphy et al., 2012b; Donahue et al., 2012a). The midpoint of the C_i^* (from the reactant C_i^* to the largest C_i^* defined in the model, $C^*_{i,\mathrm{max}}$), $C^*_{i,\mathrm{midpoint}}$, is used to distinguish heavy fragments (with volatilities lower than $C^*_{i,\mathrm{midpoint}}$) and light fragments (with volatilities higher than $C^*_{i,\mathrm{midpoint}}$). The O : C of the heavy fragments is unchanged while those of the light fragments move diagonally towards $C^*_{i,\mathrm{max}}$. Then the radical portion of the fragments is functionalized in the same way as the reactant. For example, with a radical fraction (f_{radical}) of 60 %, only 60 % of the fragments are radicals that are functionalized after the fragmentation. In this work, the first method was used in the base-case original model (OM) while the second one was also tested and compared as the modified model (MM) (see Sect. 3.3.1).

2.3 Global sensitivity analysis

The sensitivity of the base-case original 2D-VBS SOA model to 13 parameters (Table 2) was explored for one typical case with an initial gas-phase α-pinene concentration of 281 $\mu g\,m^{-3}$. Compared to the parameters listed in Table 2, other parameters associated with initial conditions (i.e., temperature, pressure, concentrations of O_3 and α-pinene) and rate coefficients of reactions of α-pinene with OH and O_3 were not included because their uncertainties are generally small (up to ±20 %, 1σ confidence level). Additional simulations confirm that varying these parameters within their uncertainties only changes modeled C_{OA} and O : C by up to 4.7 % and 0.4 %, respectively.

The ranges over which these parameters were varied are summarized in Table 2 and explained briefly below. All uncertainties in this paper are reported at 1σ confidence

ACPD
13, 2759–2793, 2013

limits. The relative error of α_i was reported to be 9 % (Pathak et al., 2007), leading to an estimated uncertainty of ±20 %. For the 2-D space of the base-case original model, n_C ranges from 3 to 26 so that the uncertainty of n_C was estimated to be ±15 %. The numbers of C_i^* bins are varied from 8 to 12, and the number of O : C bins are varied from 10 to 14 bins so that the highest C_i^* and O : C of the 2-D space are varied accordingly. Since there is generally no uncertainty assessment available for most of these parameters, perturbation ranges were assigned based on different values from previous studies or simply with broad ranges of possible values. Initial O : C ($O:C_i$) and molecular weights of first-generation oxidized products were varied within ranges of 0.2–0.5 and 150–200 g mol^{-1}, respectively, covering the reported values in Chan et al. (2009). The rate coefficients of homogeneous oxidation by OH and O_3 and heterogeneous uptake by OH were perturbed within broad ranges of (0.2–5) × 10^{-11}, (0.2–5) × 10^{-17}, and (0.2–5) × 10^{-12} cm^3 molec^{-1} s^{-1}, respectively. The fragmentation coefficient $\beta = (O:C)^{f_c}$ was varied using a range of f_c from 0.1 to 0.5. For the probability of oxygen addition during functionalization process, a broad range of 0–0.5 was assumed for both adding one (P_{1O}) and two atoms (P_{2Os}) while the probability of adding three atoms (P_{3Os}) is simply calculated by $1 - P_{1O} - P_{2Os}$.

The sensitivity of this SOA model was evaluated using a global sensitivity analysis (GSA) method by varying the values of model parameters simultaneously and quantifying their relative contribution to the modeled C_{OA} and O : C. The GSA method used here is called Random Sampling-High Dimensional Model Representation (RS-HDMR) (Li et al., 2010, and reference therein). For a model with n parameters, the sensitivity results are expressed by first-order, second-order, and higher-order sensitivity indices (S_i, S_{ij},..., $S_{12...n}$) to represent the relative contribution from individual parameter x_i, parameter pair x_i and x_j, and so forth, respectively:

$$\sum_{i=1}^{n} S_i + \sum_{1 \le i < j \le n} S_{ij} + \ldots + S_{12\ldots n} = 1. \quad (4)$$

ACPD
13, 2759–2793, 2013

The importance of x_i can hence be ranked by the total sensitivity S_{Ti}, which is defined to be the sum of all sensitivities (first-order and higher-order) involving x_i (Saltelli et al., 2008). This method has been applied in different model systems (e.g., Chen and Brune, 2012) with up to hundreds of parameters and was able to efficiently apportion the sources of model uncertainty. For this SOA model, the Monte Carlo simulations were run 1000 times with the 13 model parameters varied randomly over their uncertainty ranges and the corresponding input-output matrix was analyzed by ExploreHD (Aerodyne Inc.) to probe their impact on model results.

3 Results and discussion

3.1 Model-measurement comparison

The modeled C_{OA} and O : C ratios are compared to measurements at the same levels of OH exposure (Fig. 1). In general, half of the measured and modeled C_{OA} values agree within ±28 % and most of the data agree within ±49 %, with a correlation coefficient R of 0.79 (Fig. 1a). Larger model-measurement discrepancy (modeled-to-observed ratio ranging from 0.6 to 2.4) was observed at different levels of OH exposure for three cases with ΔVOC of 227, 695 and 833 μg m^{-3}. As shown by the typical case with ΔVOC of 281 μg m^{-3} (Fig. 1b), the model was able to reproduce the C_{OA} trend of a rapid increase at lower OH exposure followed by a slower decrease at higher OH exposure, with modeled-to-observed C_{OA} ratios of 0.9–1.3. Although the model tends to over-predict the SOA concentration at high OH exposure by a factor of ∼ 2, the model-measurement agreement is generally acceptable considering the uncertainties associated with both the experiments and modeling.

The trend in modeled O : C with respect to measured O : C is different (Fig. 1c). Modeled and measured O : C values are correlated (R = 0.68), but the trend between modeled versus measured O : C values is nonlinear. The model systematically overpredicts low O : C ratios (O : C ∼ 0.4–0.6) by as much as 53 %, and underpredicts high O : C

ACPD
13, 2759–2793, 2013

ratios (O : C ∼ 1.0–1.3) by up to 36 %. As shown by the typical case in Fig. 1d, the modeled and measured O : C values follow different trends as a function of OH exposure. The modeled O : C first increases rapidly and then more slowly, while the measured O : C increases slowly at first and then more rapidly. The possible causes of this effect will be discussed later in the paper (see Sect. 3.3).

To evaluate SOA formation at lower OH exposures than those used in the PAM chamber experiments, our base-case model was also applied to an α-pinene SOA experiment conducted in the Caltech environmental chamber (CIT) under low-NO_x conditions (Ng et al., 2007, 2010; Lambe et al., 2011). In the CIT experiment, an initial α-pinene concentration of 47.5 ppbv was used, [OH] was about 3×10^6 molec cm^{-3}, RH equaled 6.2 %, O_3 was produced from the chamber walls at a rate of ~ 1 ppbv min^{-1}, and the chamber was seeded with ammonium sulfate particles. The measured and modeled C_{OA} and O : C results of CIT are compared with the typical case of PAM in Fig. 1b and d since the ΔVOC amounts are comparable (~ 262 µg m^{-3} in CIT and 281 µg m^{-3} in PAM). The measured results with CIT and PAM conditions are broadly consistent as a function of OH exposure. Differences between other experimental conditions such as UV intensity and relative humidity (e.g., Presto et al., 2005; Pathak et al., 2007; Henry and Donahue, 2011) may contribute to any inconsistencies between CIT and PAM chamber results.

The model-measurement agreement of C_{OA} in the CIT chamber can be further improved by adjusting some parameters in the model. For example, increasing the assumed gas phase OH oxidation rate coefficient from 1×10^{-11} to 4×10^{-11} cm^3 molec^{-1} s^{-1}, which was the highest OH homogeneous rate coefficient assumed in previous VBS modeling studies (e.g., Robinson et al., 2007; Shrivastava et al., 2011), the model generally reproduces the C_{OA} in both CIT and PAM with average relative errors of 28 % and 39 %, respectively (Fig. 1b). In addition, it should be noted that the C_{OA} measurements in CIT were corrected for wall loss with first-order size-dependent coefficients (Ng et al., 2007). Therefore the uncertainty of this correction combined with experimental uncertainties in both CIT and PAM might partially explain

ACPD
13, 2759–2793, 2013

the discrepancy of the C_{OA} peaks. However, with a more recent parameterization of first-generation product yields of α-pinene oxidation (Henry et al., 2012), which are sensitive to the experimental conditions (e.g., Presto et al., 2005; Pathak et al., 2007; Henry and Donahue, 2011), the model significantly over-predicts the C_{OA} in CIT (e.g., C_{OA} peak modeled at 48 % higher than the measurement).

Figure 1d shows that the modeled O : C is overpredicted at low OH exposure in the CIT chamber as well as in the PAM chamber despite the adjustments of OH homogeneous oxidation rate coefficient and first-generation products yields. This model-measurement discrepancy of O : C is consistent with previous model results for another environmental chamber (Donahue et al., 2012a). These model adjustments also confirm that the modeled C_{OA} and O : C are highly sensitive to the model input parameters (Fig. 1b and d). In Sect. 3.3, we perform a detailed sensitivity analysis of the model parameters listed in Table 2 to provide insight into application of the 2D-VBS model to laboratory SOA measurements.

3.2 The growth and evolution of SOA

One of the advantages of the 2D-VBS is the ability to explicitly model the volatility and oxidation level (O : C) of α-pinene oxidation products as a function of OH exposure. We start by examining trends in SOA volatility distributions as a function of OH exposure in 1D-VBS space (Fig. 2), with $\Delta VOC = 443\,\mu g\,m^{-3}$. At a low OH exposure of 4×10^{10} molec cm^{-3} s, the composition of the total products C_{total} is primarily determined by the yields of first-generation products, which are mainly gas-phase intermediate volatility organic compounds (IVOCs) (Fig. 2a). The less volatile products condense into the particle phase to form SOA products, which are mostly semi-volatile organic compounds (SVOCs). As the OH exposure increases to 2.8×10^{11} molec cm^{-3} s (Fig. 2b), the α-pinene oxidation products undergo functionalization, which reduces their volatility and increases the yield of low volatility organic compounds (LVOCs) and SVOCs (Fig. 2b) so that SOA mass reaches its peak. As the OH exposure continues to increase, the SOA mass decreases slightly at 5.2×10^{11} OH cm^{-3} s (Fig. 2c) and decreases further

ACPD
13, 2759–2793, 2013

at an OH exposure of 1.3×10^{12} OH cm^{-3} s (Fig. 2d). This SOA decrease suggests an increase in the contribution of fragmentation reactions that increase product volatility and decrease the yield of LVOCs and SVOCs. The fragmentation reactions are favored by the products with higher oxidation states (Jimenez et al., 2009; Kroll et al., 2009; Lambe et al., 2012), as is evident from the increase in mass of products with $C_i^* > 1 \times 10^4$ µg m^{-3} as a function of OH exposure.

Figure 3 shows the particle-phase products from Fig. 2 plotted in 2D-VBS space (Donahue et al., 2012b). At each OH exposure, the three most abundant SOA products are shown, and in all cases contribute 74 % or more of the total particle-phase mass. We note that at each OH exposure, oxidation products with C_i^* of 10 µg m^{-3} have lower O : C than corresponding oxidation products at C_i^* of 0.1, 1, and/or 100 µg m^{-3}. This difference arises from the formation of oxidation products that have a C_i^* of 10 µg m^{-3} and come from the functionalization of the first-generation oxidation products (O : C $\sim$ 0.2, $C_i^* \sim 10^3$ µg m^{-3}) prior to subsequent evolution with increasing OH exposure.

Starting from the first-generation oxidation products (see Table 1), the modeled SOA mass and O : C ratio move with increasing OH exposure from the bottom-right hand corner to the top left-hand corner of the 2D-VBS phase space. As indicated by the carbon number and oxygen number isopleths, the average carbon number drops gradually from 10 to $\sim$ 6, while the average oxygen number increases from around 3.5 to 4.5. We note that PAM-generated SOA follows a similar 2D-VBS trajectory as ambient SOA (Jimenez et al., 2009; Donahue et al., 2012b). Thus the volatility and oxidation states of modeled and measured SOA from the photooxidation of α-pinene in the PAM chamber are generally consistent with the measured markers of SOA volatility and oxidation states in the atmosphere (Fig. 3).

3.3 Sensitivity study

As discussed in Sect. 2.2, several assumptions and simplifications have been used in this 2D-VBS model that could be responsible for the differences in the behavior of

ACPD
13, 2759–2793, 2013

measured and modeled O : C as a function of OH exposure. To investigate the influence of model configuration and model input parameters on modeled C_{OA} and O : C values, we (1) performed additional simulations using different 2D-VBS model configurations, and (2) conducted a global sensitivity analysis to determine model uncertainty and the model parameters to which the modeled C_{OA} and O : C are most sensitive. These tests could provide guidance for future model development and laboratory research.

3.3.1 Modified model configuration

An alternative model configuration (MM, see Sect. 2.2) was tested for the typical case ($\Delta VOC = 281\ \mu g\ m^{-3}$), in which lighter products of fragmentation reactions were assumed to have higher O : C than the reactants (e.g., Murphy et al., 2012b; Donahue et al., 2012a), compared to the assumption that all fragments have the same O : C as the reactants in the base-case original model (OM). Additionally, MM treats 60 % of the fragments as organic radicals that are subsequently functionalized ($f_{radical} = 60\ \%$). Compared to OM results, MM produces an average increase in both modeled C_{OA} and O : C by 21 % and 15 %, respectively, which does not improve model-measurement agreement (Fig. 4). Several parameters of MM were hence varied to probe their impact on the SOA modeling results (see Fig. 4 for selected results).

Varying one or two of the model parameters generally increase or decrease both modeled C_{OA} and O : C. For instance, we extended the number of volatility bins n_x to 13 (i.e., largest C_i^* of $10^7\ \mu g\ m^{-3}$) or the number of O : C bins n_y to 17 (i.e., largest O : C of 1.8). This change increases modeled C_{OA} by up to a factor of 2.4 and increases modeled O : C by up to 34 %. For the C_i^* axis, the modeled oxidation of the products with high C_i^* of 10^5–$10^7\ \mu g\ m^{-3}$ shifts the SOA mass in the direction of lower volatility and higher oxidation states through continuous functionalization processes. For the O : C axis, the higher O : C ratios up to 1.8 become assigned to light fragments and further functionalization can evolve the SOA to lower volatility and higher oxidation states. Another example is when $f_{radical}$ decreases from 60 % to 30 %, the modeled

ACPD
13, 2759–2793, 2013

C_{OA} and O : C are lowered on average by 53 % and 27 %, respectively. One of the parameters found to have different impacts on modeled C_{OA} and O : C is the O : C of first-generation products. Adjusting this parameter to a lower specific value (e.g., 0.2) increases the modeled C_{OA} by 43 % and decreased the modeled O : C by 13 % since more SOA mass is produced through more generations of functionalization with respect to the products with lower oxidation states.

Implementing these variations of the 2D-VBS model input parameters does not improve model-measurement agreement for C_{OA} or O : C relative to the base-case model. In many cases, the agreement is worse. However, it is possible that some model parameters need to be varied together and/or more complex scenarios are required. For instance, similar to the fragmentation coefficient β, some parameters such as the probability of adding oxygen atoms and $f_{radical}$ might change with SOA oxidation state. To improve the model-measurement agreement of C_{OA} and O : C, the global sensitivity analysis in the following section may be able to provide some insight into which model parameters are the most influential and should be examined in more detail.

3.3.2 Global sensitivity analysis

Monte Carlo simulations were conducted in which the thirteen 2D-VBS model parameters (Table 2) were simultaneously perturbed to assess the range of possible modeled C_{OA} and O : C values. Figure 5 shows the results as a function of OH exposure following 1000 Monte Carlo simulations. As expected, the range of modeled C_{OA} and O : C values (grey region) covers a significantly wider phase space than single-parameter perturbations (Sect. 3.3.1). Since some parameters such as $C^*_{i,max}$ and P_{2Os} were varied significantly from their base-case values (Table 2), the median and mean values from the Monte Carlo simulations deviate from the original model for both C_{OA} and O : C. For instance, the average modeled value of C_{OA} is up to 50 % lower than the base-case simulation of C_{OA} at high OH exposure. On the other hand, the average modeled O : C is ~ 18 % higher. A conservative model uncertainty estimate at 1σ is 40–120 % for C_{OA}

ACPD
13, 2759–2793, 2013

which inversely correlates with the SOA mass ($R = -0.89$), and ~40 % for O : C. In general, modeled and measured C_{OA} and O : C agree well within their uncertainties.

However, there are differences. For C_{OA}, the measured peak is at a slightly higher OH exposure than the modeled peak and at higher OH exposure, the measured C_{OA} is about half the modeled C_{OA} in the original model. For O : C, the difference in the shapes of curves of modeled and measured O : C vs. OH exposure is persistent and significant. A sensitivity study can provide guidance for the possible causes of these differences.

A global sensitivity analysis was performed at six OH exposures within the range of ~ (2–20) × 10^{11} molec cm^{-3} s; a summary of measurements and results from base-case modeling and Monte-Carlo simulations is shown in Table 3. The RS-HDMR method was conducted to compute up to third-order sensitivity, i.e., S_i, S_{ij}, and S_{ijk}, which represent the relative contribution from individual parameters, parameter pairs, and parameter triplets, respectively. For all of the six cases, the sums of the sensitivities ($\sum S_i + \sum S_{ij} + \sum S_{ijk}$) are greater than 0.90 (Fig. 6), indicating that over 90 % of model uncertainty can be attributed to the contribution from individual parameters and parameter pairs/triplets. The first-order sensitivity dominates with $\sum S_i > 0.62$ for C_{OA} and $\sum S_i > 0.90$ for O : C, highlighting the significant contribution of individual parameters to the model uncertainty. The sensitivities of the most important model parameters (with sensitivity greater than 0.05 for at least one case) are shown in Fig. 6.

The modeled SOA mass concentration, C_{OA}, is most sensitive to the choice of the number of C_i^* bins, n_x, especially for low OH exposure (S_i up to 0.55). This sensitivity occurs because increasing the number of bins increases $C^*_{i,max}$. When $C^*_{i,max}$ is less than 10^4 μg m^{-3}, the initial products with volatility greater than $C^*_{i,max}$ are excluded, which reduces the magnitude of semi-volatile organics that would contribute to C_{OA}. The C_{OA} sensitivity to the heterogeneous reaction rate coefficient, k_{OH_hetero}, is negligible at low OH exposure ($S_i < 0.02$), but grows to become the most important parameter at the highest OH exposure (S_i up to 0.27). This change in k_{OH_hetero} occurs because at low OH exposure, C_{OA} is primarily influenced by the initial yields of first-generation

ACPD
13, 2759–2793, 2013

oxidation products α_i (S_i up to 0.11). As the particle is further oxidized and more mass of oxidation products condenses to the particle phase, C_{OA} becomes more sensitive to the heterogeneous oxidation rate. It is interesting that the gas-phase reaction rate coefficient k_{OH_homo} has little impact on C_{OA} ($S_i < 0.03$), which implies that the gas-phase reaction rates are sufficiently fast that they do not limit the oxidation rate and thus the change in C_{OA}. C_{OA} is also sensitive to other factors, such as the probability of functionalization with two oxygens, P_{2Os}, ($S_i = 0.04$–0.09) and the initial O : C of the first-generation products (O : C_i) ($S_i = 0.02$–0.05). Note also that at higher OH exposures, C_{OA} becomes sensitive to the coupling between the n_x and k_{OH_hetero} (S_{ij} up to 0.07).

At low OH exposure, O : C is most sensitive to O : C_i (S_i up to 0.60) followed by choice of the number of C_i^* bins n_x (S_i up to 0.20), and k_{OH_homo} (S_i up to 0.12). The sensitivity of O : C to O : C_i at low OH exposure is large because O : C $\approx$ O : C_i. The sensitivity to n_x comes from different partitioning of products with different O : C between the gas phase and particle phase. The gas-phase reaction rate k_{OH_homo} is influential by increasing O : C through the functionalization process. However, at high OH exposure, O : C becomes less sensitive to these three parameters with S_i gradually decreasing to 0.15, 0.06, and 0 for O : C_i, n_x, and k_{OH_homo}, respectively. Instead, O : C becomes most sensitive to k_{OH_hetero}(S_i up to 0.33), followed by n_y (S_i up to 0.30). The increased sensitivity to n_y comes from that n_y limits the highest O : C (ranging from 1.0 to 1.4) SOA could reach as the aging process evolves SOA to higher oxidation states.

Both C_{OA} and O : C are more sensitive to k_{OH_homo} at low OH exposure, and more sensitive to k_{OH_hetero} at high OH exposure. This sensitivity shift suggests that heterogeneous reactions become more important as the SOA becomes more oxidized. SOA is initially oxidized primarily in the gas phase by OH reactions and creates semi-volatile oxidation products that partition with the particle phase, increasing C_{OA} and O : C. Further oxidation reduces the volatility of semi-volatile oxidation products so that the gas-phase concentrations of the oxidation products decrease and therefore less homogeneous oxidation can occur. As a result, heterogeneous oxidation becomes more

ACPD
13, 2759–2793, 2013

important relative to homogeneous oxidation. This result suggests that, in the atmosphere, the relative importance of heterogeneous OH reactions may increase with increasing exposure times and/or distance from sources.

4 Conclusions

Our implementation of the 2D-VBS model generally captures the observed behavior of α-pinene SOA formation and evolution in a Potential Aerosol Mass chamber and the Caltech smog chamber within the uncertainties of the model and the measurements. The modeled SOA mass concentration, C_{OA}, increases as functionalization reactions create more oxidized and less volatile VOC products and then decreases as fragmentation reactions create products that have higher volatility. In addition, the modeled SOA oxidation state, as indicated by O : C, increases in a way that is qualitatively consistent with the PAM chamber measurements. Furthermore, this modeled SOA aging is consistent with the SOA aging that is measured in the Caltech environmental chamber and in the atmosphere.

While the modeled and observed SOA O : C increase with OH exposure, the magnitude and functional form of the increase differ significantly. This difference could be due to the simple assumptions made to model the fragmentation process such as the one associated with O : C of the fragments. If this discrepancy is caused by the model, the sensitivity analysis has the potential to indicate the cause. However, none of the thousand Monte Carlo simulations were able to reproduce the measured curvature. This discrepancy is probably not due to the highly oxidizing environment in the PAM chamber because it also is seen in two large environmental chambers (Ng et al., 2007; Donahue et al., 2012a) with oxidant levels closer to ambient than that of the PAM chamber. Thus it is likely that this discrepancy emerges from the model framework.

With a global sensitivity analysis, the most important parameters for modeled C_{OA} and O : C are found to be associated with the highest C_i^* and O : C values used to define the boundary of the 2-D space, the initial mass yields and O : C ratios of the

ACPD
13, 2759–2793, 2013

products from the first-generation oxidation, particle-phase OH uptake rate and the probability of adding oxygen atoms during the functionalization process. It is possible that some of the model parameters are a function of the volatility, carbon number, molecular structure, or oxidation state of the reactant products so that the assumptions made for current model are too simplified to represent the trajectory of SOA aging accurately. Other assumptions that deserve more scrutiny include OH and O_3 reactions causing the same products or using a gas-phase reaction rate coefficient to simulate heterogeneous chemistry instead of including microphysics and well as chemistry. To examine these possibilities, this model will be compared to other models and to measurements from both the PAM chamber and large environmental chambers.

Acknowledgements. We thank A. T. Ahern, D. R. Croasdale, J. P. Wright, and P. Massoli (BC/ARI) for contributions to the laboratory experiments, D. van Duin, T. Samuelson, and K. Christian (PSU) for producing the α-pinene mixtures, O. Oluwole, C. Kolb, F. Bacon, and G. Li (ARI) for the ExplorerHD software that was used to compute global sensitivity. We also thank N. L. Ng (Georgia Tech) for Caltech chamber data. SC and WB acknowledge the support by the National Science Foundation grant AGS-0855135. ATL, PD and TBO acknowledge support by the Office of Science (BER), Department of Energy (Atmospheric Science Program) grants No. DE-SC0006980 and DE-FG02-05ER63995, and the Atmospheric Chemistry Program of the National Science Foundation grants No. ATM-0854916 and AGS-0904292.

References

Aiken, A. C., DeCarlo, P. F., Kroll, J. H., Worsnop, D. R., Huffman, J. A., Docherty, K. S., Ulbrich, I. M., Mohr, C., Kimmel, J. R., Sueper, D., Sun, Y., Zhang, Q., Trimborn, A., Northway, M., Ziemann, P. J., Canagaratna, M. R., Onasch, T. B., Alfarra, M. R., Prevot, A. S. H., Dommen, J., Duplissy, J., Metzger, A., Baltensperger, U., and Jimenez, J. L.: O/C and OM/OC Ratios of Primary, Secondary, and Ambient Organic Aerosols with High-Resolution Time-of-Flight Aerosol Mass Spectrometry, Environ. Sci. Techol., 42, 4478–4485, 2008.

Atkinson, R., Baulch, D. L., Cox, R. A., Crowley, J. N., Hampson, R. F., Hynes, R. G., Jenkin, M. E., Rossi, M. J., and Troe, J.: Evaluated kinetic and photochemical data for atmospheric

ACPD
13, 2759–2793, 2013

chemistry: Volume I – gas phase reactions of O_x, HO_x, NO_x and SO_x species, Atmos. Chem. Phys., 4, 1461–1738, doi:10.5194/acp-4-1461-2004, 2004.

Aumont, B., Szopa, S., and Madronich, S.: Modelling the evolution of organic carbon during its gas-phase tropospheric oxidation: development of an explicit model based on a self generating approach, Atmos. Chem. Phys., 5, 2497–2517, doi:10.5194/acp-5-2497-2005, 2005.

Bahreini, R., Middlebrook, A. M., Brock, C. A., de Gouw, J. A., McKeen, S. A., Williams, L. R., Daumit, K. E., Lambe, A. T., Massoli, P., Canagaratna, M. R., Ahmadov, R., Carrasquillo, A. J., Cross, E. S., Ervens, B., Holloway, J. S., Hunter, J. F., Onasch, T. B., Pollack, I. B., Roberts, J. M., Ryerson, T. B., Warneke, C., Davidovits, P., Worsnop, D. R., and Kroll, J. H.: Mass spectral analysis of organic aerosol formed downwind of the deepwater horizon oil spill: Field studies and laboratory confirmations, Environ. Sci. Technol., 46, 8025–8034, 2012.

Chan, M. N., Chan, A. W. H., Chhabra, P. S., Surratt, J. D., and Seinfeld, J. H.: Modeling of secondary organic aerosol yields from laboratory chamber data, Atmos. Chem. Phys., 9, 5669–5680, doi:10.5194/acp-9-5669-2009, 2009.

Chen, S. and Brune, W. H.: Global sensitivity analysis of ozone production and O_3-NO_x-VOC limitation based on field data, Atmos. Environ., 55, 288–296, 2012.

Cappa, C. D. and Wilson, K. R.: Multi-generation gas-phase oxidation, equilibrium partitioning, and the formation and evolution of secondary organic aerosol, Atmos. Chem. Phys., 12, 9505–9528, doi:10.5194/acp-12-9505-2012, 2012.

Chacon-Madrid, H. J. and Donahue, N. M.: Fragmentation vs. functionalization: chemical aging and organic aerosol formation, Atmos. Chem. Phys., 11, 10553–10563, doi:10.5194/acp-11-10553-2011, 2011.

Chacon-Madrid, H. J., Murphy, B. N., Pandis, S. N., and Donahue, N. M.: Simulations of smog-chamber experiments using the two-dimensional volatility basis set, Linear oxygenated precursors, Environ. Sci. Technol., 46, 11179–11186, 2012.

DeCarlo, P. F., Kimmel, J. R., Trimborn, A., Northway, M. J., Jayne, J. T., Aiken, A. C., Gonin, M., Fuhrer, K., Horvath, T., Docherty, K. S., Worsnop, D. R., and Jimenez, J. L.: Field-deployable, High-resolution, Time-of-Flight Aerosol Mass Spectrometer, Anal. Chem., 78, 8281–8289, 2006.

Donahue, N. M., Robinson, A. L., Stanier, C. O., and Pandis, S. N.: Coupled partitioning, dilution, and chemical aging of semivolatile organics, Environ. Sci. Technol., 40, 2635–2643, 2006.

ACPD
13, 2759–2793, 2013

Donahue, N. M., Epstein, S. A., Pandis, S. N., and Robinson, A. L.: A two-dimensional volatility basis set: 1. organic-aerosol mixing thermodynamics, Atmos. Chem. Phys., 11, 3303–3318, doi:10.5194/acp-11-3303-2011, 2011.

Donahue, N. M., Henry, K. M., Mentel, T. F., Kiendler-Scharr, A., Spindler, C., Bohn, B., Brauers, T., Dorn, H. P., Fuchs, H., Tillmann, R., Wahner, A., Saathoff, H., Naumann, K.-H., Möhler, O., Leisner, T., Müller, L., Reinnig, M.-C., Hoffmann, T., Salo, K., Hallquist, M., Frosch, M., Bilde, M., Tritscher, T., Barmet, P., Praplan, A. P., DeCarlo, P. F., Dommen, J., Prévôt, A. S. H., and Baltensperger, U.: Aging of biogenic secondary organic aerosol via gas-phase OH radical reactions, Proc. Natl. Acad. Sci. USA, 109, 13503–13508, 2012a.

Donahue, N. M., Epstein, S. A., Pandis, S. N., and Robinson, A. L.: A two-dimensional volatility basis set: 1. organic-aerosol mixing thermodynamics, Atmos. Chem. Phys., 11, 3303–3318, doi:10.5194/acp-11-3303-2011, 2011b.

Drewnick, F., Hings, S. S., DeCarlo, P., Jayne, J. T., Gonin, M., Fuhrer, K., Weimer, S., Jimenez, J. L., Demerjian, K. L., Borrmann, S., and Worsnop, D. R.: A new Time-of-Flight Aerosol Mass Spectrometer (TOF-AMS)–Instrument description and first field deployment, Aerosol Sci. Technol., 39, 637–658, 2005.

Dzepina, K., Volkamer, R. M., Madronich, S., Tulet, P., Ulbrich, I. M., Zhang, Q., Cappa, C. D., Ziemann, P. J., and Jimenez, J. L.: Evaluation of recently-proposed secondary organic aerosol models for a case study in Mexico City, Atmos. Chem. Phys., 9, 5681–5709, doi:10.5194/acp-9-5681-2009, 2009.

El Haddad, I., D'Anna, B., Temime-Roussel, B., Nicolas, M., Boreave, A., Favez, O., Voisin, D., Sciare, J., George, C., Jaffrezo, J.-L., Wortham, H., and Marchand, N.: On the chemical nature of the oxygenated organic aerosol: implication in the formation and aging of α-pinene SOA in a Mediterranean environment, Marseille, Atmos. Chem. Phys. Discuss., 12, 19769–19797, doi:10.5194/acpd-12-19769-2012, 2012.

EPA: Our nation's air – Status and trends through 2010, US Environmental Protection Agency, Office of Air Quality Planning and Standards, Research Triangle Park, North Carolina, 2012.

Guenther, A., Hewitt, C. N., Erickson, D., Fall, R., Geron, C., Graedel, T., Harley, P., Klinger, L., Lerdau, M., McKay, W. A., Pierce, T., Scholes, B., Steinbrecher, R., Tallamraju, R., Taylor, J., and Zimmerman, P.: A global model of natural volatile organic compound emissions, J. Geophys. Res., 100, 8873–8892, 1995.

Hallquist, M., Wenger, J. C., Baltensperger, U., Rudich, Y., Simpson, D., Claeys, M., Dommen, J., Donahue, N. M., George, C., Goldstein, A. H., Hamilton, J. F., Herrmann, H., Hoffmann,

ACPD
13, 2759–2793, 2013

T., Iinuma, Y., Jang, M., Jenkin, M. E., Jimenez, J. L., Kiendler-Scharr, A., Maenhaut, W., McFiggans, G., Mentel, T. F., Monod, A., Prévôt, A. S. H., Seinfeld, J. H., Surratt, J. D., Szmigielski, R., and Wildt, J.: The formation, properties and impact of secondary organic aerosol: current and emerging issues, Atmos. Chem. Phys., 9, 5155–5236, doi:10.5194/acp-9-5155-2009, 2009.

Henry, K. M. and Donahue, N. M.: Effect of the OH radical scavenger hydrogen peroxide on secondary organic aerosol formation from α-pinene ozonolysis, Aerosol Sci. Technol., 45, 696–700, 2011.

Henry, K. M., Lohaus, T., and Donahue, N. M.: Organic aerosol yields from α-pinene oxidation: Bridging the gap between first-generation yields and aging chemistry, 46, 12347–12354, Environ. Sci. Technol., 2012.

Jathar, S. H., Miracolo, M. A., Presto, A. A., Donahue, N. M., Adams, P. J., and Robinson, A. L.: Modeling the formation and properties of traditional and non-traditional secondary organic aerosol: problem formulation and application to aircraft exhaust, Atmos. Chem. Phys., 12, 9025–9040, doi:10.5194/acp-12-9025-2012, 2012.

Jimenez, J. L., Canagaratna, M. R., Donahue, N. M., Prevot, A. S. H., Zhang, Q., Kroll, J. H., DeCarlo, P. F., Allan, J. D., Coe, H., Ng, N. L., Aiken, A. C., Docherty, K. S., Ulbrich, I. M., Grieshop, A. P., Robinson, A. L., Duplissy, J., Smith, J. D., Wilson, K. R., Lanz, V. A., Hueglin, C., Sun, Y. L., Tian, J., Laaksonen, A., Raatikainen, T., Rautiainen, J., Vaattovaara, P., Ehn, M., Kulmala, M., Tomlinson, J. M., Collins, D. R., Cubison, M. J., E., Dunlea, J., Huffman, J. A., Onasch, T. B., Alfarra, M. R., Williams, P. I., Bower, K., Kondo, Y., Schneider, J., Drewnick, F., Borrmann, S., Weimer, S., Demerjian, K., Salcedo, D., Cottrell, L., Griffin, R., Takami, A., Miyoshi, T., Hatakeyama, S., Shimono, A., Sun, J. Y., Zhang, Y. M., Dzepina, K., Kimmel, J. R., Sueper, D., Jayne, J. T., Herndon, S. C., Trimborn, A. M., Williams, L. R., Wood, E. C., Middlebrook, A. M., Kolb, C. E., Baltensperger, U., and Worsnop, D. R.: Evolution of organic aerosols in the atmosphere, Science, 326, 1525–1529, 2009.

Kang, E., Root, M. J., Toohey, D. W., and Brune, W. H.: Introducing the concept of Potential Aerosol Mass (PAM), Atmos. Chem. Phys., 7, 5727–5744, doi:10.5194/acp-7-5727-2007, 2007.

Kroll, J. H., Chan, A. W. H., Ng, N. L., Flagan, R. C., and Seinfeld, J. H.: Reactions of Semivolatile Organics and Their Effects on Secondary Organic Aerosol Formation, Environ. Sci. Tech., 41, 3545–3550, 2007.

ACPD
13, 2759–2793, 2013

Kroll, J. H., Smith, J. D., Che, D. L., Kessler, S. H., Worsnop, D. R., and Wilson, K. R.: Measurement of fragmentation and functionalization pathways in the heterogeneous oxidation of oxidized organic aerosol, Phys. Chem. Chem. Phys., 11, 8005–8014, 2009.

Kroll, J. H., Donahue, N. M., Jimenez, J. L., Kessler, S. H., Canagaratna, M. R., Wilson, K. R., Altieri, K. E., Mazzoleni, L. R., Wozniak, A. S., Bluhm, H., Mysak, E. R., Smith, J. D., Kolb, C. E., and Worsnop, D. R.: Carbon oxidation state as a metric for describing the chemistry of atmospheric organic aerosol, Nat. Chem., 3, 133–139, 2011.

Lambe, A. T., Ahern, A. T., Williams, L. R., Slowik, J. G., Wong, J. P. S., Abbatt, J. P. D., Brune, W. H., Ng, N. L., Wright, J. P., Croasdale, D. R., Worsnop, D. R., Davidovits, P., and Onasch, T. B.: Characterization of aerosol photooxidation flow reactors: heterogeneous oxidation, secondary organic aerosol formation and cloud condensation nuclei activity measurements, Atmos. Meas. Tech., 4, 445–461, doi:10.5194/amt-4-445-2011, 2011.

Lambe, A. T., Onasch, T. B., Croasdale, D. R., Wright, J. P., Martin, A. T., Franklin, J. P., Massoli, P., Kroll, J. H., Canagaratna, M. R., Brune, W. H., Worsnop, D. R., and Davidovits, P.: Transitions from functionalization to fragmentation reactions of laboratory secondary organic aerosol (SOA) generated from the OH oxidation of alkane precursors, 46, 5430–5437, Environ. Sci. Technol, 2012.

Lane, T. E., Donahue, N. M., and Pandis, S. N.: Simulating secondary organic aerosol formation using the volatility basis-set approach in a chemical transport model, Atmos. Environ., 42, 7439–7451, 2008.

Li, G., Rabitz, H., Yelvington, P. E., Oluwole, O. O., Bacon, F., Kolb, C. E., and Schoendorf, J.: Global sensitivity analysis for systems with independent and/or correlated inputs, J. Phys. Chem., 114, 6022–6032, 2010.

Mao, J., Ren, X., Brune, W. H., Olson, J. R., Crawford, J. H., Fried, A., Huey, L. G., Cohen, R. C., Heikes, B., Singh, H. B., Blake, D. R., Sachse, G. W., Diskin, G. S., Hall, S. R., and Shetter, R. E.: Airborne measurement of OH reactivity during INTEX-B, Atmos. Chem. Phys., 9, 163–173, doi:10.5194/acp-9-163-2009, 2009.

Massoli, P., Lambe, A. T., Ahern, A. T., Williams, L. R., Ehn, M., Mikkilä, J., Canagaratna, M. R., Brune, W. H., Onasch, T. B., Jayne, J. T., Petäjä, T., Kulmala, M., Laaksonen, A., Kolb, C. E., Davidovits, P., and Worsnop, D. R.: Relationship between aerosol oxidation level and hygroscopic properties of laboratory generated secondary organic aerosol (SOA) particles, Geophys. Res. Lett., 37, L24801, doi:10.1029/2010GL045258, 2010.

ACPD
13, 2759–2793, 2013

Murphy, B. N., Donahue, N. M., Fountoukis, C., and Pandis, S. N.: Simulating the oxygen content of ambient organic aerosol with the 2D volatility basis set, Atmos. Chem. Phys., 11, 7859–7873, doi:10.5194/acp-11-7859-2011, 2011.

Murphy, B. N., Donahue, N. M., Fountoukis, C., Dall'Osto, M., O'Dowd, C., Kiendler-Scharr, A., and Pandis, S. N.: Functionalization and fragmentation during ambient organic aerosol aging: application of the 2-D volatility basis set to field studies, Atmos. Chem. Phys., 12, 10797–10816, doi:10.5194/acp-12-10797-2012, 2012.

Ng, N. L., Chhabra, P. S., Chan, A. W. H., Surratt, J. D., Kroll, J. H., Kwan, A. J., McCabe, D. C., Wennberg, P. O., Sorooshian, A., Murphy, S. M., Dalleska, N. F., Flagan, R. C., and Seinfeld, J. H.: Effect of NOx level on secondary organic aerosol (SOA) formation from the photooxidation of terpenes, Atmos. Chem. Phys., 7, 5159–5174, doi:10.5194/acp-7-5159-2007, 2007.

Ng, N. L., Canagaratna, M. R., Zhang, Q., Jimenez, J. L., Tian, J., Ulbrich, I. M., Kroll, J. H., Docherty, K. S., Chhabra, P. S., Bahreini, R., Murphy, S. M., Seinfeld, J. H., Hildebrandt, L., Donahue, N. M., DeCarlo, P. F., Lanz, V. A., Prévôt, A. S. H., Dinar, E., Rudich, Y., and Worsnop, D. R.: Organic aerosol components observed in Northern Hemispheric datasets from Aerosol Mass Spectrometry, Atmos. Chem. Phys., 10, 4625–4641, doi:10.5194/acp-10-4625-2010, 2010.

Odum, J. R., Hoffmann, T., Bowman, F., Collins, D., Flagan, R. C., and Seinfeld, J. H.: Gas/Particle partitioning and secondary organic aerosol yields, Environ. Sci. Technol., 30, 2580–2585, 1996.

Pankow, J. F.: An absorption model of the gas/aerosol partitioning involved in the formation of secondary organic aerosol, Atmos. Environ., 28, 189–193, 1994.

Pankow, J. F. and Asher, W. E.: SIMPOL.1: a simple group contribution method for predicting vapor pressures and enthalpies of vaporization of multifunctional organic compounds, Atmos. Chem. Phys., 8, 2773–2796, doi:10.5194/acp-8-2773-2008, 2008.

Pathak, R. K., Presto, A. A., Lane, T. E., Stanier, C. O., Donahue, N. M., and Pandis, S. N.: Ozonolysis of α-pinene: parameterization of secondary organic aerosol mass fraction, Atmos. Chem. Phys., 7, 3811–3821, doi:10.5194/acp-7-3811-2007, 2007.

Presto, A. A., Huff Hartz, K. E., and Donahue, N. M.: Secondary organic aerosol production from terpene ozonolysis, 1, Effect of UV radiation, Environ. Sci. Technol., 39, 7036–7045, 2005.

ACPD
13, 2759–2793, 2013

Robinson, A. L., Donahue, N. M., Shrivastava, M. K., Weitkamp, E. A., Sage, A. M., Grieshop, A. P., Lane, T. E., Pierce, J. R., and Pandis, S. N.: Rethinking organic aerosols: semivolatile emissions and photochemical aging, Science, 315, 1259–1262, 2007.

Roldin, P., Swietlicki, E., Schurgers, G., Arneth, A., Lehtinen, K. E. J., Boy, M., and Kulmala, M.: Development and evaluation of the aerosol dynamics and gas phase chemistry model ADCHEM, Atmos. Chem. Phys., 11, 5867–5896, doi:10.5194/acp-11-5867-2011, 2011.

Sander, S. P., Abbatt, J., Barker, J. R., Burkholder, J. B., Friedl, R. R., Golden, D. M., Huie, R. E., Kolb, C. E., Kurylo, M. J., Moortgat, G. K., Orkin, V. L., and Wine, P. H.: Chemical Kinetics and Photochemical Data for Use in Atmospheric Studies, Evaluation No. 17, JPL Publication 10-6, Jet Propulsion Laboratory, Pasadena, 2011, http://jpldataeval.jpl.nasa.gov, 2011.

Shrivastava, M., Fast, J., Easter, R., Gustafson Jr., W. I., Zaveri, R. A., Jimenez, J. L., Saide, P., and Hodzic, A.: Modeling organic aerosols in a megacity: comparison of simple and complex representations of the volatility basis set approach, Atmos. Chem. Phys., 11, 6639–6662, doi:10.5194/acp-11-6639-2011, 2011.

Spracklen, D. V., Jimenez, J. L., Carslaw, K. S., Worsnop, D. R., Evans, M. J., Mann, G. W., Zhang, Q., Canagaratna, M. R., Allan, J., Coe, H., McFiggans, G., Rap, A., and Forster, P.: Aerosol mass spectrometer constraint on the global secondary organic aerosol budget, Atmos. Chem. Phys., 11, 12109–12136, doi:10.5194/acp-11-12109-2011, 2011.

Stanier, C. O., Pathak, R. K., and Pandis, S. N.: Measurements of the volatility of aerosols from α-pinene ozonolysis, Environ. Sci. Technol., 41, 2756–2763, 2007.

Stanier, C.O., Donahue, N., and Pandis, S. N.: Parameterization of secondary organic aerosol mass fractions from smog chamber data, Atmos. Environ., 42, 2276–2299, 2008.

Wagstrom, K. M. and Pandis, S. N.: Determination of the age distribution of primary and secondary aerosol species using a chemical transport model, J. Geophys. Res., 114, D14303, doi:10.1029/2009JD011784, 2009.

Yu, S., Bhave, P. V., Dennis, R. L., and Mathur, R.: Seasonal and regional variations of primary and secondary organic aerosols over the continental United States: semi-26 empirical estimates and model evaluation, Environ. Sci. Technol., 41, 4690–4697, 2007.

ACPD
13, 2759–2793, 2013

Table 1. The initial O : C and mass yields α_i of VBS products from the oxidation of α-pinene.

C_i^* ($\mu g\,m^{-3}$)	α_i	O : C	Molecular Weight ($g\,mol^{-1}$)
10^0	0.024	0.4	200
10^1	0.078	0.3	184
10^2	0.060	0.45	150
10^3	0.222	0.2	168
10^4	0.770	0.45	150
Reference	Pathak et al. (2007)	Chan et al. (2009), Lambe et al. (2011)	Chan et al. (2009), Pathak et al. (2007)

ACPD
13, 2759–2793, 2013

Table 2. The perturbation ranges and sampling probability distribution function (PDF) of model parameters of this SOA model.

#	Parameter	Original Value	Perturbation range	PDF	Ref.
1	Initial RH	20 % for lower RH cases; 30 % for higher RH cases	20–25 % for lower RH cases; 30–40 % for higher RH cases	uniform	This work
2	Number of C_i^* bins n_x	10	8–12 (10^{-5} to 10^{2} or 10^{6} μg m^{-3})	uniform integers	This work
3	Number of O : C bins n_y	12	10–14 (0.1 to 1.0 or 1.4)	uniform integers	This work
4	Molecular weight of first-generation products	See Table 1	150–200 g mol^{-1}	uniform	Chan et al. (2009)
5	Homogeneous k_{OH_homo}	1×10^{-11} cm^3 s^{-1}	$(0.2–5)\times10^{-11}$ cm^3 s^{-1}	uniform	This work
6	Homogeneous k_{O_3}	1×10^{-17} cm^3 s^{-1}	$(0.2–5) \times 10^{-17}$ cm^3 s^{-1}	uniform	This work
7	Heterogeneous k_{OH_hetero}	1×10^{-12} cm^3 s^{-1}	$(0.2–5) \times 10^{-12}$ cm^3 s^{-1}	uniform	This work
8	Initial O : C of first-generation products	See Table 1	0.2-0.5	uniform	Chan et al. (2009)
9	Product yields of first-generation products α_i	See Table 1	±20 %	normal	This work
10	Carbon number of grouped products n_C	Calculated from Donahue et al. (2011)	±15 %	uniform	This work
11	f_c of fragmentation coefficient $\beta = (O:C)^{f_c}$	1/6	0.1-0.5	uniform	This work
12	Adding 2Os probability P_{1O}	29 %	0–0.5	uniform	This work
13	Adding 2Os probability P_{2Os}	49 %	0–0.5	uniform	This work
–	Adding 3Os probability P_{3Os}	22 %	$1\text{-}P_{1O}\text{-}P_{2Os}$	–	This work

ACPD
13, 2759–2793, 2013

Table 3. The variations of modeled SOA and OH exposure (OHexp) as a result of 1000 Monte Carlo simulations for the six cases with different OH exposure levels.

#	Measurement			Model		Monte Carlo Simulations		
	OH_{exp} (molec cm^{-3} s)	O : C	C_{OA} ($\mu g\,m^{-3}$)	O : C	C_{OA} ($\mu g\,m^{-3}$)	OH_{exp} (molec cm^{-3} s)	O : C	C_{OA} ($\mu g\,m^{-3}$)
1	1.6×10^{11}	0.40	116	0.58	92	$(1.7 \pm 0.3) \times 10^{11}$	0.68 ± 0.16	100 ± 63
2	3.8×10^{11}	0.44	125	0.67	98	$(4.2 \pm 0.6) \times 10^{11}$	0.81 ± 0.16	87 ± 63
3	6.7×10^{11}	0.50	113	0.74	86	$(7.1 \pm 1.1) \times 10^{11}$	0.89 ± 0.16	68 ± 58
4	1.0×10^{12}	0.66	81	0.79	71	$(1.1 \pm 0.2) \times 10^{12}$	0.96 ± 0.16	51 ± 52
5	1.4×10^{12}	0.85	43	0.84	56	$(1.5 \pm 0.3) \times 10^{12}$	1.02 ± 0.16	36 ± 47
6	2.1×10^{12}	1.11	12	0.90	39	$(2.1 \pm 0.4) \times 10^{12}$	1.07 ± 0.16	24 ± 39

ACPD
13, 2759–2793, 2013

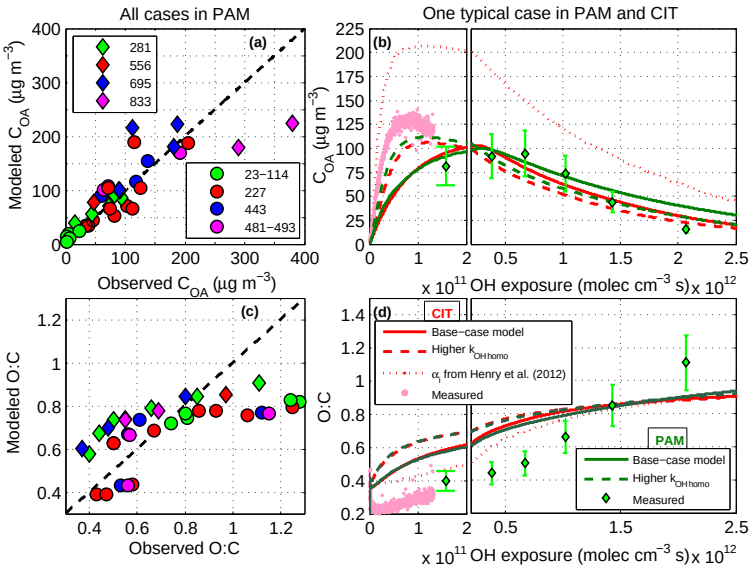

Fig. 1. The comparison of modeled and measured C_{OA} (upper panel) and O : C (lower panel) for all cases with different initial conditions of PAM chamber (initial α-pinene concentrations (ΔVOC) are shown in the legends with unit of μg m^{-3}; circles denote the results from RH = 20–25 % and O_3 = 8 ppmv cases and diamonds denote the results from RH = 30–40 % and O_3 = 20 ppmv cases) and one typical case with ΔVOC of 281 μg m^{-3} (the errorbars denote the 1σ uncertainty of the measurements). The measurements of C_{OA} are calculated from the averages of AMS and SMPS measurements. The measured C_{OA} and O : C in Caltech's environmental chamber (CIT) with comparable ΔVOC (262 μg m^{-3}) (Ng et al., 2007) are also shown for comparison in **(b)** and **(d)**, respectively, while the modeling results are simulated based on the CIT conditions with base-case model and adjusted model parameters (see the text). Note that different scaling of OH exposure is used for x-axis in **(b)** and **(d)** to show the results at lower and higher OH exposure levels.

ACPD
13, 2759–2793, 2013

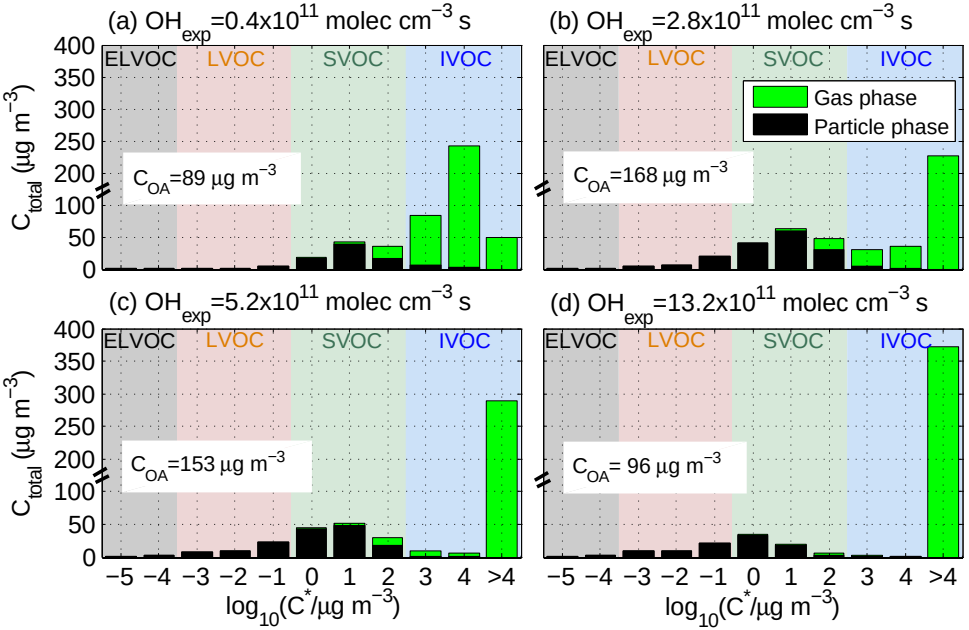

Fig. 2. The modeled variation of the volatility of the products generated from the oxidation of α-pinene in the PAM chamber. Initial conditions: ΔVOC = 443 µg m^{-3}, RH = 20 %, O_3 = 8 ppmv. The mass of products with $C_i^* > 10^4$ µg m^{-3} were calculated based on carbon mass conservation and were assumed to stay in gas phase and not participate in further oxidation. The volatility classes of organics defined by Donahue et al. (2012b) are used here.

ACPD
13, 2759–2793, 2013

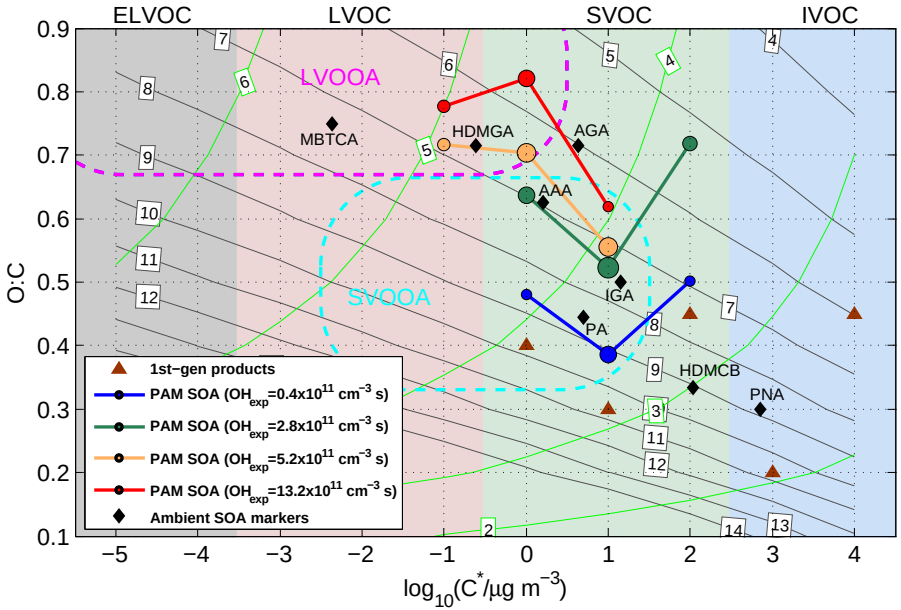

Fig. 3. The evolution of particle-phase mass and O : C simulated from the oxidation of α-pinene (ΔVOC = 443 μg m^{-3}). The 2D-VBS space, classes of VOCs and OOA, and the contours (grey: carbon numbers; green: oxygen numbers) are adapted from Donahue et al. (2012b). The circles show the three most abundant products grouped in different volatility bins (contributing over 74 % to the total SOA mass) for each of four levels of OH exposure in Fig. 2. The size of each circle indicates the relative particle-phase mass of the bulk products (see Fig. 2). The black diamonds denote the markers of ambient SOA from the photooxidation of α-pinene: pinonic acid (PNA), 3-(2-hydroxyethyl)-2,2- dimethylcyclobutane carboxylic acid (HDMCB), pinic acid (PA), 3-isopropylglutaric acid (IGA), 3-acetyladipic acid (AAA), 3-acetylglutaric acid (AGA), 3-hydroxy-4,4- dimethylglutaric acid (HDMGA), and 3-methyl-1,2,3-butanetricarboxylic (MBTCA) (El Haddad et al., 2012 and references therein). The volatility of these markers were estimated at 298 K based on SIMPOL method (Pankow and Asher, 2008).

ACPD
13, 2759–2793, 2013

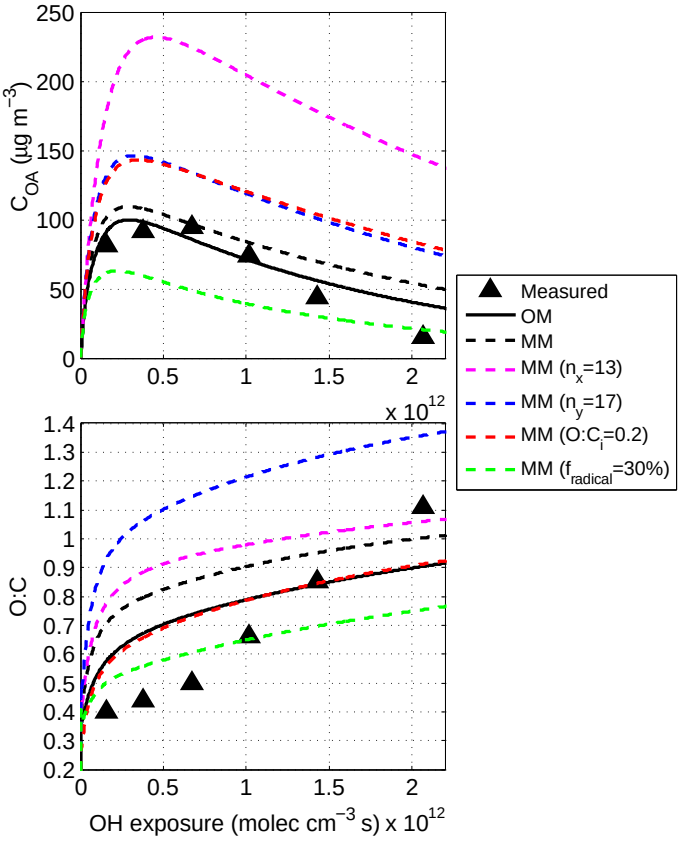

Fig. 4. The modeled result of C_{OA} and O : C from both the original model (OM, denoted by solid lines) and modified model (MM, denoted by dash lines) (Murphy et al., 2012b; Donahue et al., 2012a) with the initial α-pinene of 281 μg m^{-3} when some parameters are varied (see legend).

ACPD
13, 2759–2793, 2013

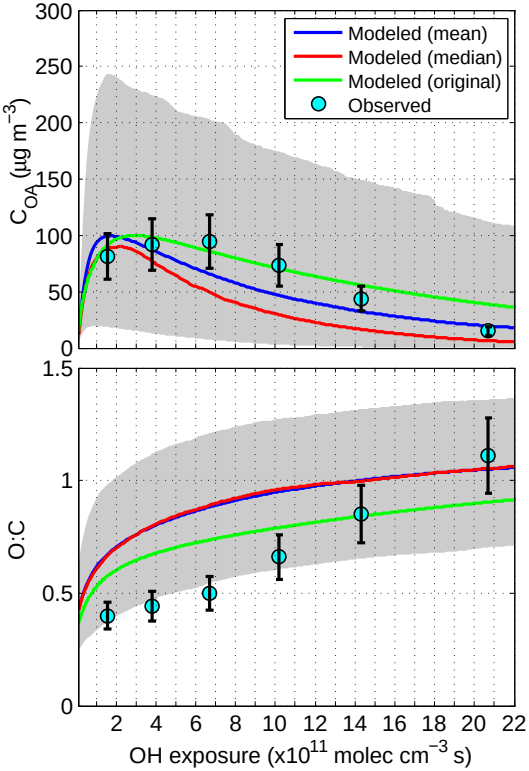

Fig. 5. The variation of modeled C_{OA} and O : C resulting from the variation of model parameters of the base-case original model for the case with initial α-pinene of 281 μg m^{-3} . The gray shadow extends to the most extreme data points corresponding to 97.5 and 2.5 percentiles, that is, 95 % coverage of the data. The error bars show the uncertainties of measured COA and O : C.

ACPD
13, 2759–2793, 2013

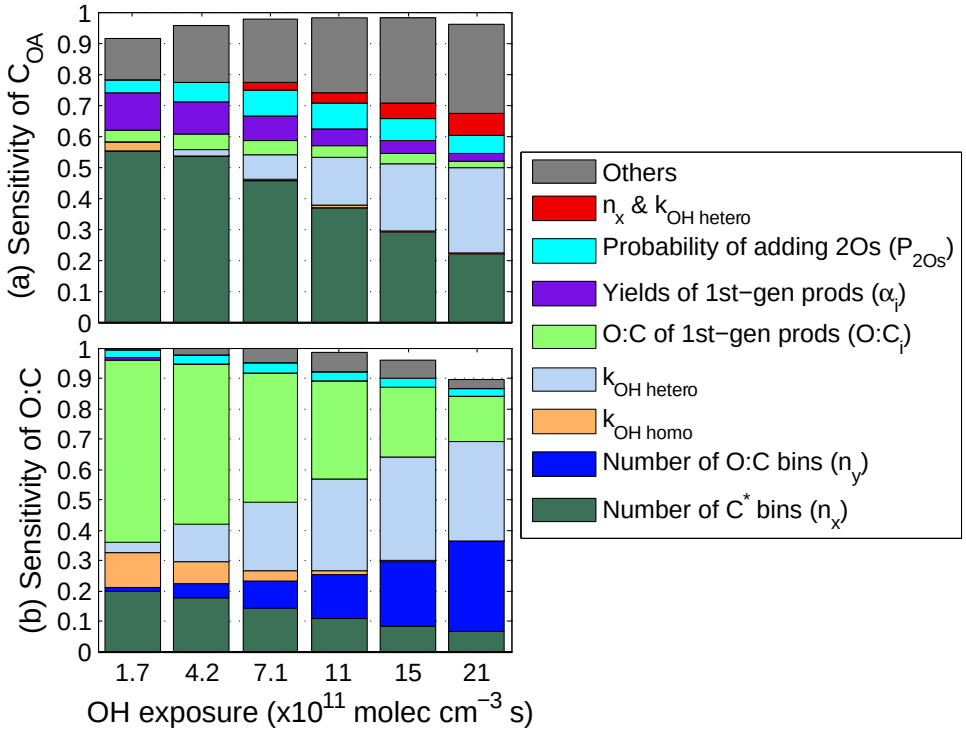

Fig. 6. The sensitivity of modeled **(a)** C_{OA} and **(b)** O : C for the six cases that represent the evolution of SOA at different OH exposure levels of (2–20) × 10^{11} molec cm^{-3} s. Only important model parameters (sensitivity greater than 0.05 for at least one case) are shown here.

ACPD
13, 2759–2793, 2013